



Research Article

Shaking Table Test Study on the Earthquake Behavior of High-Speed Railway Bridge Pier with Rounded Rectangular Cross Section

Xin Kang ¹, Yongjian Zuo ^{2,3}, Leqiao Zeng,¹ Linna Peng,¹ Qiliang Wang,¹ Xiaoxiang Wang,¹ Libin Deng,¹ Jia Hu,¹ Zhuo Li,¹ and Likun Li⁴

¹Hunan Construction Investment Group Co. LTD, Changsha 410075, China

²School of Civil Engineering, Central South University, Changsha 410075, China

³National Engineering Laboratory for High Speed Railway Construction, Changsha 410075, China

⁴China MCC22 Group Corporation LTD, Tangshan 063000, China

Correspondence should be addressed to Yongjian Zuo; 204812240@csu.edu.cn

Received 23 May 2022; Accepted 13 August 2022; Published 6 September 2022

Academic Editor: Wonseok Chung

Copyright © 2022 Xin Kang et al. This is an open access article distributed under the Creative Commons Attribution License, which permits unrestricted use, distribution, and reproduction in any medium, provided the original work is properly cited.

Rounded rectangular cross section piers were widely used for high-speed railway (HSR) bridges in China. However, the performance of such piers under seismic scenarios has not been well studied. To study the earthquake behavior and damage of rounded rectangular cross section piers under different intensities of earthquake excitation, nine scaled pier specimens were constructed and tested on the shaking table. Experimental results show that the specimen remains elastic (no or slight damaged) for all experimental earthquake scenarios (from 0.45 g to 0.96 g). Finite element (FE) models were developed and validated by the experimental results. Using this FE model, the damage levels of these specimens under severe earthquake excitations (from 1.05 g to 1.95 g) were quantified. Numerical results show that the specimen in transverse direction shows no or slight damage, while repairable damage can be seen in longitudinal direction as the earthquake intensity increases from 1.05 g to 1.65 g. Repairable and unreparable damage can be seen in transverse and longitudinal direction, respectively, as the earthquake intensity increases to 1.95 g. Researchers can make good use of these findings for better earthquake design or protection of this type of HSR piers in the future.

1. Introduction

For bridges, the pier plays a significant role in resisting seismic force under an earthquake excitation. Therefore, its seismic performance and damage level need to be well studied (experimentally and numerically) to ensure whole structural safety [1,2,3]. Nowadays, there are many experiments conducted to examine the earthquake behavior of piers and some of these focused on the piers with rectangular section. For example, Pinto et al. [4] performed cyclic tests on two large-scale models of existing reinforced concrete (RC) bridge piers to study their seismic performance and failure modes. Chung et al. [5] carried out a quasistatic test on 6 fibre reinforced polymer (FRP) confined reinforced concrete bridge piers to evaluate their seismic performance

and failure modes. Han et al. [6] conducted cyclic test on 5 pier specimens to investigate the seismic performance of reinforced concrete (RC) bridge piers. Yeh et al. [7] studied the seismic performance by conducting cyclic tests on 3 prototype piers. Xia et al. [8] carried out biaxial quasistatic tests on 14 reinforced concrete thin-walled piers and the seismic properties were studied in detail.

In addition, there are also many experimental researches about the piers with circular section. For example, Shim et al. [9] performed quasistatic tests on precast segmental bridge piers to investigate the seismic behavior of this type of pier. Wang et al. [10] manufactured 8 partially concrete-filled steel circular bridge pier specimens and studied their seismic performance by cyclic test. Osada et al. [11] carried out static and pseudodynamic tests on circular reinforced concrete

(RC) bridge piers to study their seismic performance. Yuan et al. [12] conducted cyclic test to investigate the seismic performance of partially concrete-filled steel tube (PCFST) bridge piers with circular section by cyclic test.

Apart from experimental methods, validated finite element (FE) analysis has also been applied for detailed parametric analysis. For example, Dong et al. [13] proposed a simplified FE model, validated by test results, to evaluate the seismic performance of fibre reinforced polymer (FRP) confined reinforced concrete rectangular bridge piers. Lee et al. [14] developed and experimentally validated a multidimensional fiber-based section model, which offers accuracy and computational efficiency to study the seismic performance of rectangular section reinforced concrete (RC) piers. Guo et al. [15] proposed a simplified mechanical model to study the seismic performance of a self-centering bridge pier and the results were validated by quasistatic test. Sun et al. [16] experimentally studied the seismic performance of reinforced concrete bridge piers and established a validated finite element model to study the hysteretic behavior of pier.

Due to the need to increase train speed, high-speed railway bridges (HSRBs) are increasingly constructed. For the HSRBs, the piers with rounded rectangular cross section are widely applied, since it provides larger stiffness in the transverse direction and prevents stress concentrations when compared to those circular and rectangular sections. However, researches about the seismic performance and damage of this type of HSRB piers are limited. As the loading (high-speed train) to the HSRB piers is quite different in nature to that of conventional piers (with rectangular or circular section), the results (experimentally and numerically) from abovementioned studies cannot be directly applied for this typical pier for the following reasons. Firstly, to ensure the comfort and stability of high-speed train travel, a larger sectional size is common for HSRB piers. Since the larger sectional size can result in a larger bending stiffness (EI), the seismic performance of this type of pier is different to those common piers (with rectangular or circular section). Moreover, HSRB piers generally have a lower longitudinal reinforcement percentage compared to other piers, which also result in a different seismic performance. Therefore, specifically targeted experimental studies are necessary for this type of HSRB pier [17].

To achieve a better understanding of the earthquake behavior and damage level of HSRB piers with rounded rectangular cross section, shaking table tests and numerical analysis were conducted in this paper. Specifically, nine scaled pier specimens were fabricated in accordance with specific similarity relations and tested on the shake table. During the test, acceleration, displacement, and strain of each pier under the peak ground acceleration (PGA) scale of 0.45 g, 0.60 g, and 0.96 g (simulate the Chinese common earthquakes (0.15 g, 0.20 g, and 0.32 g) after similarity transformation) were recorded. Moreover, the change of natural frequency before and after each test scenario was also obtained. Secondly, a finite element (FE) model of this specimen was also established and validated against the experiments. Using this model, the damage of these pier

specimens under earthquake excitations was quantified. The results from this work can benefit for understanding the seismic performance of HSRB piers with rounded rectangular cross section and for providing suggestions on their earthquake safety assessment.

2. Shaking Table Test

2.1. Materials. All materials used for the construction of pier specimen (e.g., rebar and concrete) were the same as those of the prototype HSRB piers. Specifically, grade HRB 235, 335 steel and grade C35 concrete (according to Chinese code GB50010-2010) were used for longitudinal rebar and concrete, respectively. To obtain the material properties, three concrete blocks ($100 \times 100 \times 300$ mm) were prepared for concrete compressive strength test. For example, the design value of compressive strength $f_{cu,k}$, the compressive strength f_{cu} and the axial compressive strength f_c were given in Table 1. Diameters of 8 mm and 10 mm rebar were used in this test and their average yield strengths were 452 MPa and 405 MPa, respectively. Plain steel rebar of 6 mm diameter was used as transverse reinforcement with the yield strength of 550 MPa.

2.2. Specimens. Due to the limitation of acceleration capacity (no more than PGA scale of 1.0 g) and size of shake table (no more than 4 (length) \times 4 (width) m^2), the prototype pier should be scaled for shaking table tests. Therefore, an experimental specimen should be conducted for shaking table test and reflects the dynamic characteristics (or earthquake behavior) of corresponding prototype pier. The key of designing shaking table test programme is to determine the similarity relationship between the scaled specimen and prototype [18,19,20]. In this study, dimensional analysis was applied in this experiment to determine the similarity relationship of physical quantities between the actual HSRB pier and specimen. To be specific, the ratio of $E/\rho al$ should be kept the same for the specimen and prototype bridge, where E , ρ , a , and l represent the elastic modulus, density, acceleration, and length parameters, respectively. In this work, the geometric (S_l) was selected as 1/8 (for 16 and 24 m prototype piers) and 1/5 (for 8 m prototype piers). The acceleration (S_a) of the specimen was 3, while the elastic modulus ratio (S_E) was 1 since the same materials were applied in both specimen and prototype pier. Other remaining ratios, for example, stress, displacement, and stiffness were determined from these three basic ratios according to the similarity relations as shown in Tables 2 and 3. Detailed sectional geometries of the specimens are shown in Figure 1 [21].

Furthermore, in order to meet the similarity requirement for additional density in specimen, a steel container for weights was constructed and installed on the top of specimens, which filled with leads. These weights acted as additional dead load and inertial forces to meet the similarity requirement to the prototype bridge. Moreover, they can also represent the axial compression ratio from girder and therefore, this arrangement can simulate the true seismic

TABLE 1: Compressive strength of concrete (average value).

Specimen	$f_{cu,k}$ (MPa)	f_{cu} (MPa)	f_c (MPa)
M1, M2, M3	35	43.1	28.8
M4, M5, M6	35	43.4	26.7
M7, M8, M9	35	38.6	25.2

TABLE 2: Similitude parameters of the shaking table test for 8 m piers.

Property	Physical quantity	Similarity relation	Ratio
Material	Modulus*	S_E	1
	Stress	$S_\sigma = S_E$	1
	Density	$S_\rho = S_\sigma / S_a S_l$	5/3
Load	Point load	$S_p = S_E S_l^2$	1/25
	Line load	$S_\omega = S_E S_l$	1/5
	Area load	$S_q = S_E$	1
Geometric	Length*	S_l	1/5
	Displacement	$S_d = S_l$	1/5
	Area	$S_A = S_l^2$	1/25
Dynamic	Acceleration*	S_a	3
	Mass	$S_m = S_\rho S_l^3$	1/125
	Period	$S_T = S_l (S_\rho S_E^{-1})^{0.5}$	$\sqrt{1/15}$

TABLE 3: Similitude parameters of the shaking table test for 16 and 24 m piers.

Property	Physical quantity	Similarity relation	Ratio
Material	Modulus*	S_E	1
	Stress	$S_\sigma = S_E$	1
	Density	$S_\rho = S_\sigma / S_a S_l$	8/3
Load	Point load	$S_p = S_E S_l^2$	1/64
	Line load	$S_\omega = S_E S_l$	1/8
	Area load	$S_q = S_E$	1
Geometric	Length*	S_l	1/8
	Displacement	$S_d = S_l$	1/8
	Area	$S_A = S_l^2$	1/64
Dynamic	Acceleration*	S_a	3
	Mass	$S_m = S_\rho S_l^3$	1/192
	Period	$S_T = S_l (S_\rho S_E^{-1})^{0.5}$	$\sqrt{1/24}$

behavior of prototype pier in the actual situation. In addition, screw bolts were used to ensure no relative displacement occurred between the weights and steel container during the shaking table test. The final assembled specimen for shaking table tests is as shown in Figure 2.

2.3. Instrumentation. Acquisition devices (e.g., accelerometers and linear variable displacement transducers) were installed at the top of specimen to collect the time histories responses of acceleration and displacement in both the x (longitudinal) and y (transverse) directions during the shaking table tests, as shown in Figure 3.

2.4. Test Scenarios. The high-speed railway bridges built in China were usually excited by the earthquakes with characteristic periods ranged from 0.1 s to 0.4 s. Therefore, for better simulating representative earthquakes, and to easily

compare to other relevant studies, the El-Centro wave (characteristic periods ranged from 0.1 s to 0.4 s) was selected from the Pacific Earthquake Engineering Research (PEER) centre ground motion database. Because the acceleration limit of the shake table is no more than 1.00 g, the maximum intensity of experimental earthquake was selected as 0.96 g for this test. After the similarity transformation ($S_a = 3$, Table 2), the PGA scale of experimental earthquake intensity was adjusted to 0.45 g, 0.60 g, and 0.96 g, respectively. They correspond to simulate the actual earthquake excitation of 0.15 g, 0.20 g, and 0.32 g PGA, which are frequent happening earthquake intensities in China. An example of the recorded time history and spectrum for the of 0.45 g PGA earthquake (in the x and y directions) is illustrated in Figures 4 and 5, respectively. Moreover, the specimen was also subjected to low-amplitude white noise excitation (PGA scale of 0.05 g) to monitor the change in dynamic characteristics before and after being subjected to seismic excitations. Table 4 gives the details of the test scenarios.

3. Test Results and Discussion

3.1. Natural Frequency. To understand the seismic damage state of this specimen after being subjected to each experimental earthquake scenario, one method is to compare the change in its first natural frequency. This is because the change of specimen stiffness can be reflected by the decrease of frequency (specifically, $\omega = \sqrt{K/M}$). Therefore, to obtain the change of natural frequency of specimen between each test, a white noise excitation of 0.05 g PGA was applied to excite the specimen both before and after the earthquake excitation. The sampling frequency (f_s) and duration of white noise (T) were 500 Hz and 120 seconds, respectively. After applying the Fast Fourier Transform (*FFT*) to the recorded acceleration time histories, the natural frequency of the pier specimens was obtained. Figure 6 illustrates the first natural frequency of the specimen before and after being subjected to different earthquake intensities in both x and y directions. It shows clearly that the change of natural frequency is insignificant. To be more specific, the first natural frequency cumulatively changed from about 4.4 Hz (before any seismic excitation) to 4.1 Hz (after the 0.96 g earthquake excitation) in the x direction and from around 9.6 Hz to 8.8 Hz in the y direction. Therefore, it is reasonable to conclude from the experimental results that the specimens remain elastic region (or slight damaged) after being subjected to all the experimental excitations (i.e., 0.45 g, 0.60 g, and 0.96 g) and can withstand more severe earthquake excitations, namely, beyond 0.96 g for the scaled pier specimen or 0.32 g for the prototype pier (linked to the similarity relationship, Table 2). Moreover, as the decrease of first natural frequency in y direction (8.3%) is larger than that in x direction (6.8%), the specimens would be more easily damaged (or influenced) in y direction by an earthquake.

3.2. Acceleration. As noted earlier, the acceleration time histories under different earthquake excitations (i.e., 0.45 g,

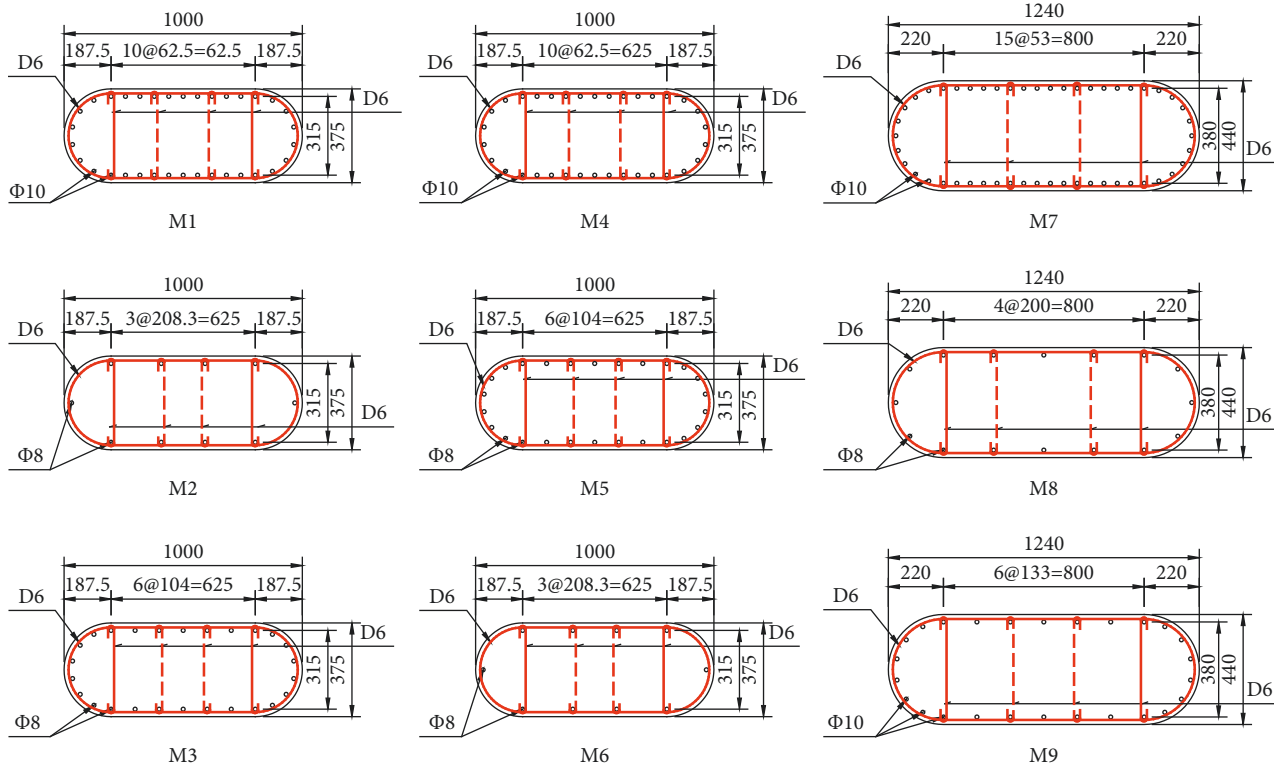


FIGURE 1: Drawings for specimen (unit: cm).

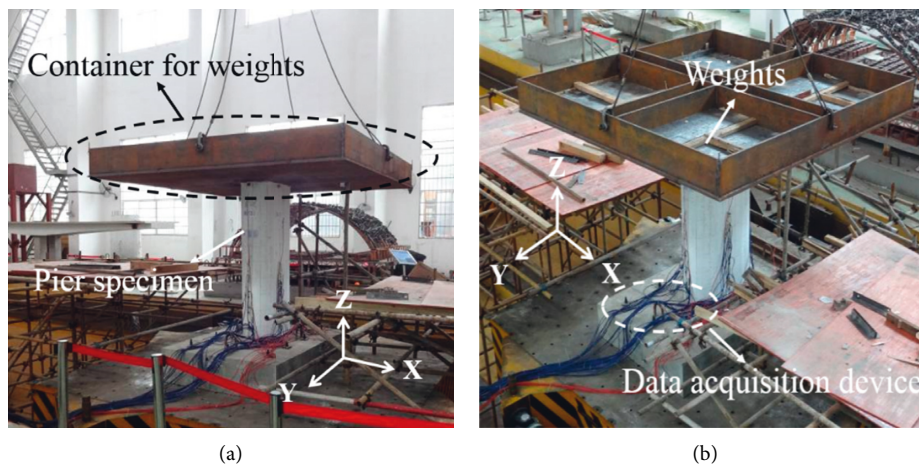


FIGURE 2: Assembled experimental pier specimen.

0.60 g, and 0.96 g) were recorded during the tests. For example, Figure 7 shows the acceleration time histories (in both x and y direction) which was obtained from the specimen subjected to the 0.45 g earthquake excitation. As can be seen from this figure, the maximum absolute acceleration value in y direction (1.10 g) was about twice as that in x direction (0.57 g). This can be ascribed to the fact that the bending stiffness of specimen in y directions is (EI_y) larger than that in x direction (EI_x) and therefore, the specimens are more effected by y direction earthquake.

Furthermore, since the seismic force ($F=MA$) to the specimen increases with increase of earthquake intensity, an

increasing trend of acceleration response can also be seen at the top of this specimen (in both x and y directions). Specifically, the maximum absolute acceleration value increases from about 0.78 g (x direction) and 1.25 g (y direction) under 0.60 g PGA excitation to 1.11 g (x direction) and 1.65 g (y direction) under 0.96 g PGA excitation. From these results, it can be seen that similar ratios between the acceleration in y and x direction (the maximum absolute acceleration in y direction is about twice as that in x direction) are also observed for the specimen when subjected to the higher earthquake intensities (from 0.60 g to 0.96 g). This result is expected since, as discussed in Section 3.1, the

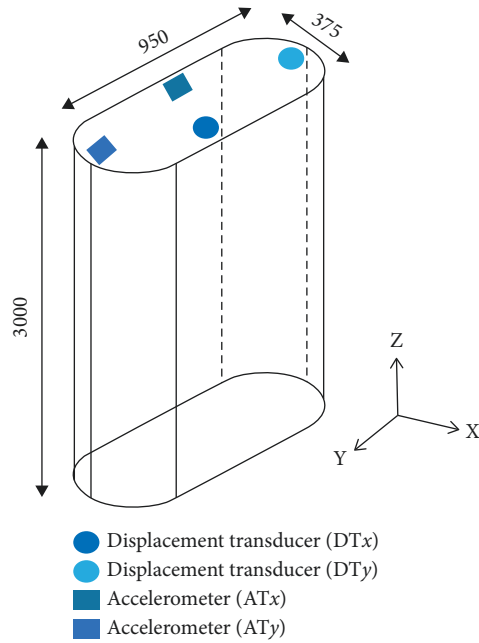


FIGURE 3: Instrumentation of data acquisition devices for experimental pier specimen (unit: mm).

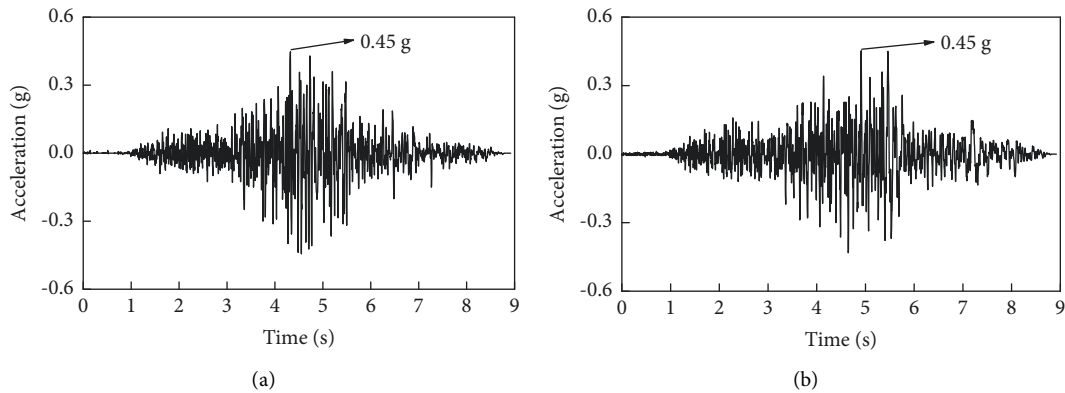


FIGURE 4: Shaking table test used waves for (a) in (x) direction and (b) in (y) direction.

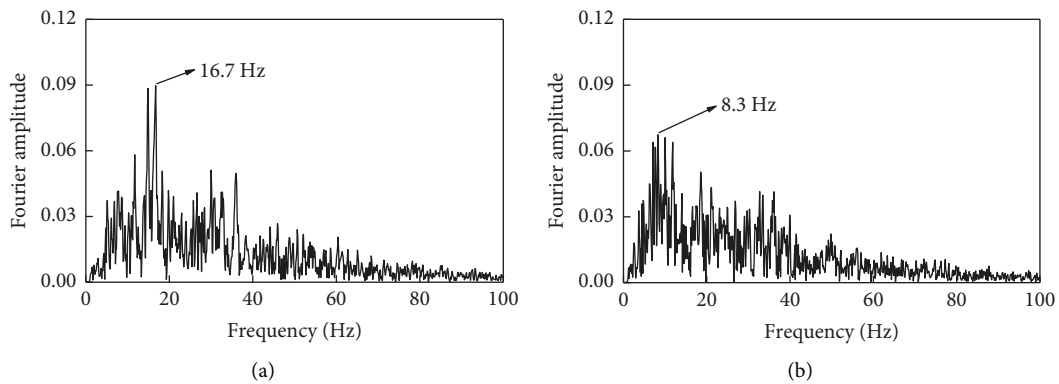


FIGURE 5: Earthquake wave spectrum for (a) in (x) direction and (b) in (y) direction.

specimens were found to remain in the elastic region (slight damaged) for all experimental earthquakes, and linear increase in acceleration response can be seen in the specimens with the increase of earthquake intensity.

3.3. Displacement. The measured displacements at the top of the specimen (in both x and y directions) when subjected to different earthquake intensities (0.45 g, 0.60 g, and, 0.96 g) are discussed in this section. As an example, Figure 8 shows

TABLE 4: Sequence of the shaking table test scenarios.

Test scenario	Prototype intensity	Test intensity (g)	
		x direction	y direction
1	White noise	0.05	0.05
2	0.15 g	0.45	N.A.
3		N.A.	0.45
4	White noise	0.05	0.05
5	0.20 g	0.60	N.A.
6		N.A.	0.60
7	White noise	0.05	0.05
8	0.32 g	0.96	N.A.
9		N.A.	0.96
10	White noise	0.05	0.05

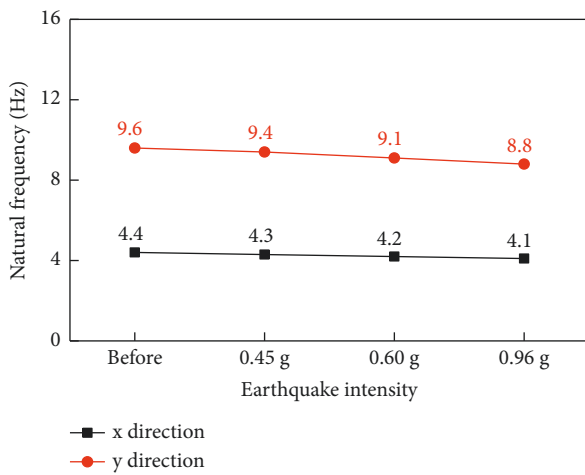


FIGURE 6: First natural frequency of pier specimen before and after under different experimental earthquake excitations.

the displacement time histories for the x and y directions when subjected to the PGA scale of 0.45 g experimental earthquake excitation. Similar to the acceleration response, the maximum absolute displacement value in y direction (about 5.89 mm) is larger than that in x direction (about 2.51 mm).

A similar trend in displacement responses was also observed for the specimen under severe intensity of earthquake excitations (from 0.60 g to 0.96 g). Specifically, the maximum absolute displacement values increased with increasing earthquake intensity, from about 3.01 mm (x direction) and 6.80 mm (y direction) at 0.60 g PGA to around 3.54 mm (x direction) and 7.90 mm (y direction) at 0.96 g PGA. Interestingly, the increase of displacement between different experimental earthquake intensities (e.g., from 0.45 g to 0.60 g and from 0.60 g to 0.96 g) is almost the same (specifically, about 0.50 mm and 1.00 mm for x and y directions, respectively). Therefore, the increase of displacement appears linear, supporting the earlier finding that the specimens remain elastic (slight damaged) and that no unrecoverable displacement occurred at the top of specimen during all earthquake excitations.

4. FE Modelling

For more detailed study about the hysteresis behavior and damage level of the specimens, FE model was developed using OpenSEES [22] and validated by the results of shaking table test. In this section, the modelling process, analysis procedure, and validation are documented.

4.1. Modelling Process. For FE model, the mass of each node (located at every 300 mm along the specimen) was taken as half of total mass of its associated elements. The mass of additional weights was included on the top of node (black solid dot in Figure 9(a)). Moreover, a lumped mass matrix was formulated in this FE model for a more efficient calculation. For better simulation of the dynamic characteristics of specimen under earthquake excitation, fibre section was selected to model the sectional restoring force (hysteretic model) of specimen. To be specific, each section was divided into a number of fibres including unconfined concrete, confined concrete, and reinforcement fibre. Therefore, the restoring force-deformation relationship of each section can be modelled from the stress-strain relations of each fibre. For each fibre section, Concrete 02, which considered the tensile mechanical property and deterioration of stiffness in unloading [23, 24], was used as the constitutive relationship for both unconfined and confined concrete [25]. Moreover, Steel 02 (Giuffre-Menegotto-Pinto model with isotropic strain-hardening) and Kent-Scott-Park concrete material (Concrete 02) [26] were applied for the constitutive relationship of rebar and concrete. Confined concrete (Table 5), unconfined concrete (Table 6), and rebar (Table 7) used in the FE modelling were all obtained from material tests.

For the element, the specimen was modelled by nonlinear beam-column elements and this type of element allows the various element stiffness along the vertical direction (z direction; see Figure 3). Specifically, the resistance force and tangent stiffness matrix of each element can be integrated from resistance force and stiffness matrix of fibre section along the vertical direction according to the Gauss-Lobatto integration method. The element flexibility matrix can be expressed as in (1). Finally, they were 10 elements for this specimen and each element had 2 integration points. The distribution of nodes and detailed fibre section of the FE model are shown in Figure 9.

$$[f]^e = \int_L [N(x)^T] [f(x)]^e [N(x)] dx. \quad (1)$$

4.2. Analysis Procedure. For the solution of the nonlinear equations of motion, the energy increment test in *OpenSees* was applied to determine the convergence at each iteration. The convergence criterion was set as 1.0×10^{-8} kNm and the maximum number of iterations was 10. For nonlinear dynamic analysis, different algorithms (e.g., Newton-Raphson, modified Newton-Raphson, Broyden and Newton with line searching algorithm) were applied if unsatisfactory convergence was found. Moreover, Newmark-beta integration

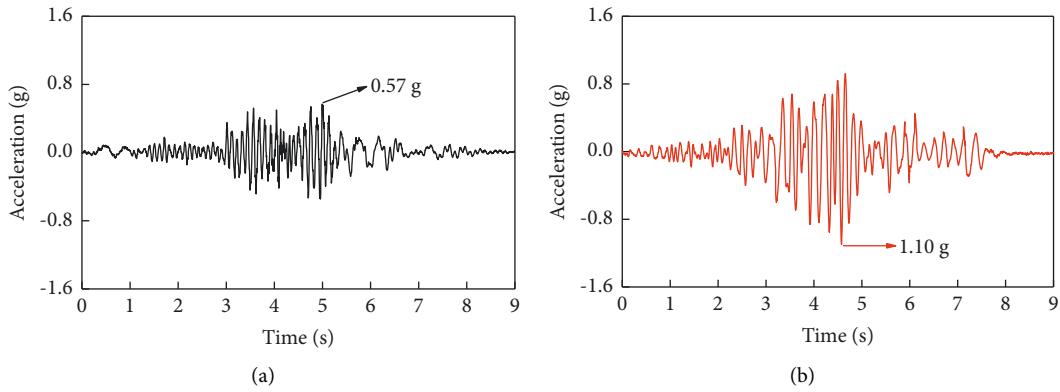


FIGURE 7: Acceleration time history at the top of specimen for (a) (x) direction and (b) (y) direction under 0.45 g experimental earthquake excitation.

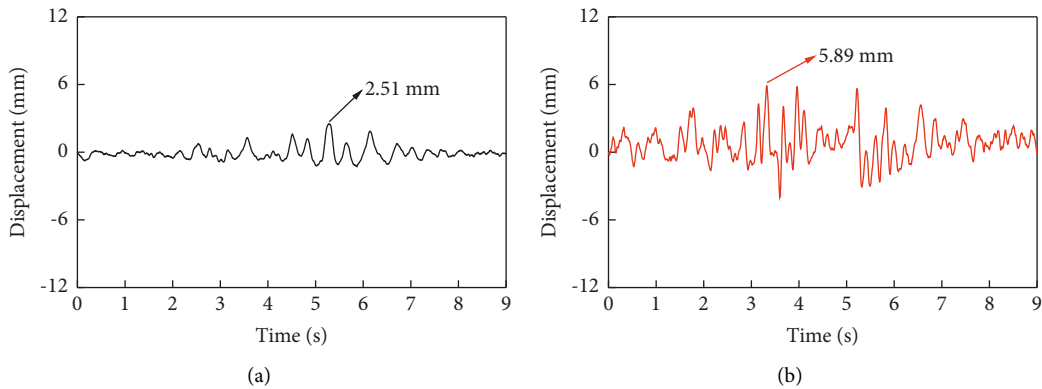


FIGURE 8: Displacement at the top of specimen for (a) (x) direction and (b) (y) direction at 0.45 g earthquake excitation.

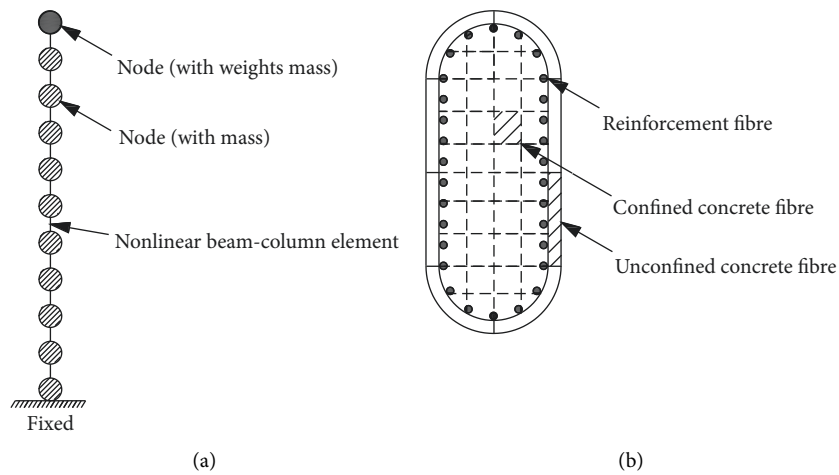


FIGURE 9: (a) Element model. (b) Fibre section of the experimental pier specimen.

TABLE 5: Parameter values of confined concrete used in FE modelling.

Compressive strength	Strain at maximum strength	Crushing strength
$30.50 e^6$	$3.50 e^{-3}$	$24.40 e^6$
Crushing strain	Tensile strength	Tension softening stiffness
$18.18 e^{-3}$	$1.57 e^6$	$2.00 e^4$

TABLE 6: Parameter values of unconfined concrete used in FE modelling.

Compressive strength	Strain at maximum strength	Crushing strength
$30.50e^6$	$3.50e^{-3}$	$5.08e^6$
Crushing strain	Tensile strength	Tension softening stiffness
$18.18e^{-3}$	$1.57e^6$	$2.00e^4$

TABLE 7: Parameter values of rebar used in FE modelling.

Yield strength	Initial elastic tangent	Strain-hardening ratio
$390.9e^6$	$2.0e^{11}$	0.01
R0	CR1	CR2
18	0.925	0.15

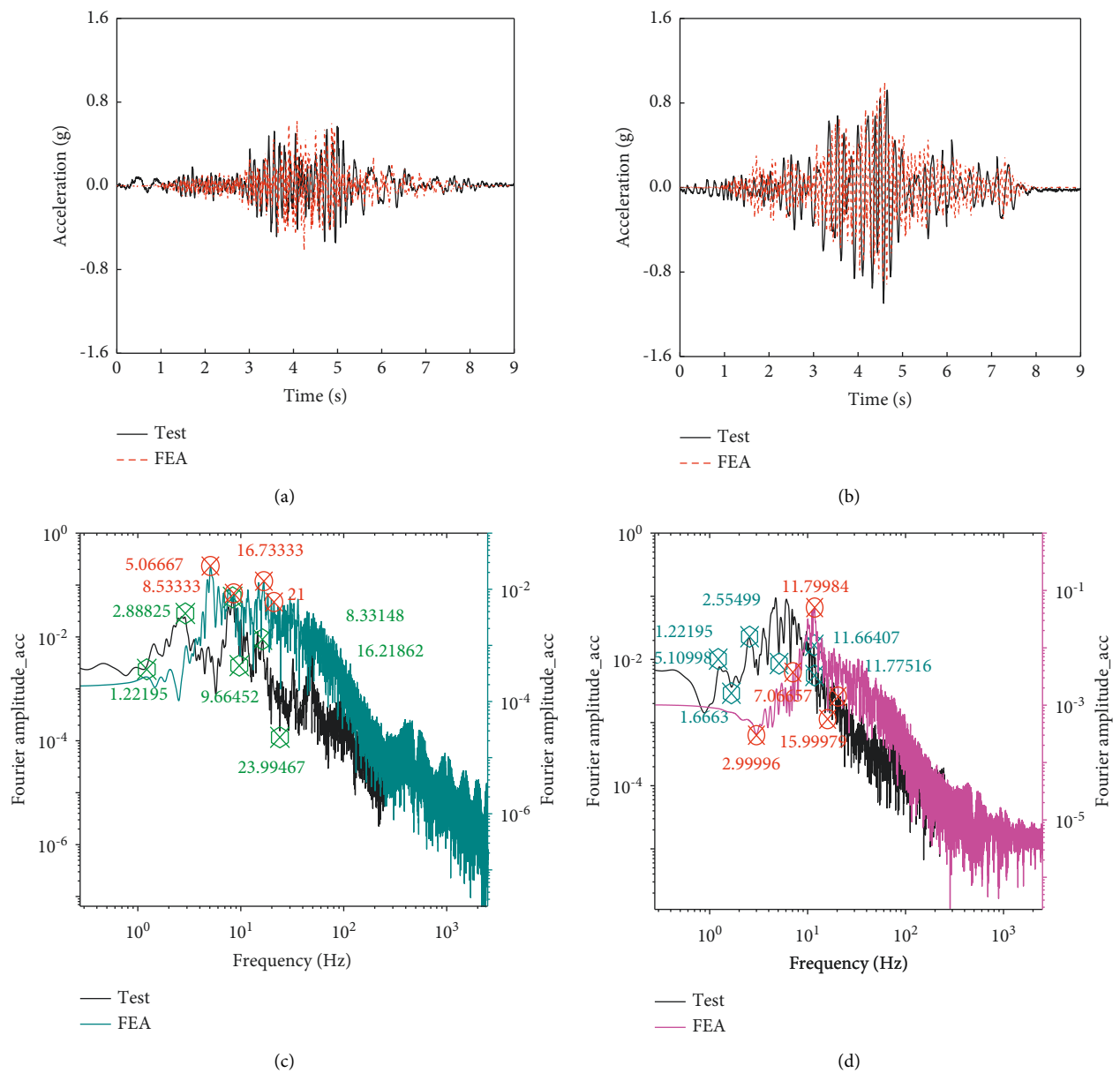


FIGURE 10: Acceleration time histories comparison under 0.45 g excitation: (a) in x direction; (b) in y direction. Fourier spectrum corresponding to (a). (d) Fourier spectrum corresponding to (b).

TABLE 8: Comparison of maximum absolute acceleration and displacement between the FE model and test under different earthquake excitations.

Results	Intensity (g)	Direction	FE model	Test	Error (%)
Acceleration (g)	0.45	<i>x</i>	0.54	0.57	5.56
		<i>y</i>	1.06	1.10	3.77
	0.60	<i>x</i>	0.71	0.78	9.86
		<i>y</i>	1.24	1.25	0.81
	0.96	<i>x</i>	1.08	1.11	2.78
		<i>y</i>	1.59	1.65	3.77
Displacement (mm)	0.45	<i>x</i>	2.33	2.51	7.72
		<i>y</i>	5.33	5.89	10.51
	0.60	<i>x</i>	2.66	3.01	13.16
		<i>y</i>	6.14	6.80	10.75
	0.96	<i>x</i>	3.38	3.54	4.73
		<i>y</i>	7.32	7.90	7.92

Note. Error = (test result–FE model result)/FE model result \times 100%.

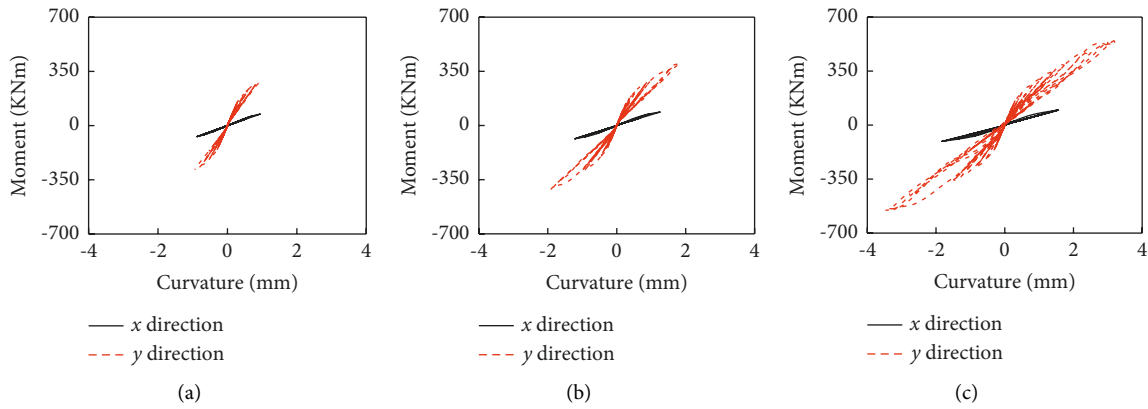


FIGURE 11: Sectional hysteresis behavior at the bottom of specimen under (a) 0.45 g, (b) 0.60 g, and (c) 0.96 g PGA earthquakes.

(average acceleration parameters: $\gamma = 1/2$, $\beta = 1/4$) method was adopted. The damping matrix in the equations of motion was formed using a proportional (Rayleigh) damping assumption, with constants defined using the 1st and 3rd mode frequencies. In addition, the damping ratio was obtained by free vibration test of this specimen. To be specific, the damping ratio can be calculated by the following equation:

$$\zeta = \frac{1}{2\pi} \ln \frac{a_1}{a_2}, \quad (2)$$

where a_1 and a_2 refer to the acceleration amplitude of specimen observed at free vibration test between two adjacent peak points.

4.3. Modelling Validation. To validate the FE model, the results of shaking table test and FE modelling are compared in this section. For example, the comparisons of acceleration time histories and Fourier spectrum (in both *x* and *y* directions) when subjected to the 0.45 g PGA earthquake excitation are illustrated in Figure 10. It can be seen that the comparison results show reasonable agreement. For more detailed validation, the maximum absolute values (acceleration and displacement) between the shaking table

test and FE modelling calculation for all earthquake excitations (from the 0.45 g to 0.96 g PGA) are given in Table 8. The comparison results show that the maximum differences in accelerations and displacements are acceptable (about 9.9% and 13.2%, respectively). Therefore, the FE model is validated and can be applied for more detailed study reported in the following sections.

5. Numerical Results and Discussion

Through the validated FE model, more detailed seismic performance (i.e., hysteresis behavior) and damage level of specimens when subjected to the earthquakes (PGA scale of 0.45 g, 0.60 g, and 0.96 g) were investigated.

5.1. Hysteresis Behavior. The hysteresis behavior (bending moment-curvature relations) at the bottom section of specimen when subjected to these earthquakes is illustrated in Figure 11. It can be seen that the hysteresis loops in *x* and *y* directions become larger and plumper with the increase of earthquake intensity (from 0.45 g to 0.96 g). This result can be reasonably explained by the fact that the seismic force ($F = MA$) to the specimen is increases correspondingly with the earthquake intensity. However, the hysteresis loops in *x*

TABLE 9: Salient points in the moment-curvature relationships for the piers.

Direction	Yield curvature Φ_y ($\times 10^{-3}/m$)	Yield moment M_y (KNm)	Limit curvature Φ_u ($\times 10^{-3}/m$)
x	8.81	172.27	198.22
y	3.48	366.82	77.38

TABLE 10: Energy consumption of the pier in x and y directions.

PGA (g)	0.45	0.60	0.96
$\int dE_x$	545.7	773.7	1361.6
$\int dE_y$	7680.1	9151.5	16042.8

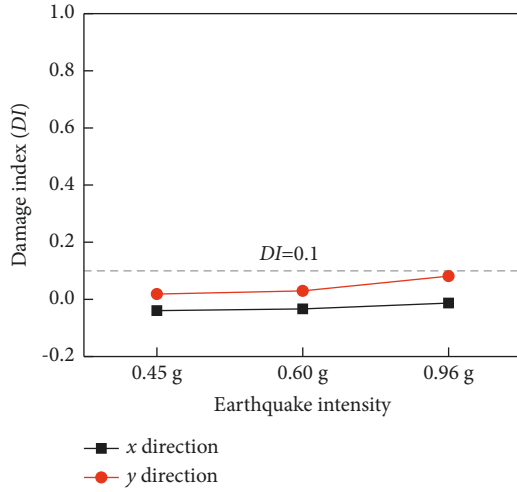


FIGURE 12: Variation of specimen damage indices with earthquake intensity.

direction are almost straight line (Figure 11), which illustrates that the specimens remain in the elastic region (slight damaged) in x direction when subjected to all analysed earthquakes. In contrast, a small plump hysteretic loop can be seen in the y direction at 0.45 g PAG excitation and this loop widens as the earthquake intensity increases to 0.96 g PGA. Therefore, the results show that the specimen in y direction is easier damaged.

5.2. Earthquake Damage Level. The damage index proposed by Stone and Taylor [27] was applied for better describing the earthquake damage level of this specimen when subjected to the earthquake excitations (PGA from 0.45 g to 0.96 g). This index is calculated as

$$DI = \frac{\Phi_m - \Phi_y}{\Phi_u - \Phi_y} + \beta_e \frac{\int dE}{M_y \Phi_u}, \quad (3)$$

where DI is the damage index; Φ_m is the maximum curvature of pier under earthquake excitation; Φ_y is the yielding curvature of pier under monotonic loading; Φ_u is the limit curvature of pier under monotonic loading; M_y is the yield moment of pier under monotonic loading; β_e is the energy factor of structure, and $\int dE$ is the cumulative hysteretic energy consumption of the pier after subjected to earthquake excitation. For calculating the damage index, the values of Φ_y , Φ_u , and M_y are given in Table 9 and the

value of $\int dE$ is shown in Table 10. Based on [16], there are four damage states corresponding to different damage indices. Specifically, there are (1) no (slight) damage ($DI < 0.10$); (2) repairable damage ($0.10 < DI < 0.40$); (3) unreparable damage ($0.40 < DI < 0.77$); and (4) collapse damage ($0.77 < DI < 1.0$).

Figure 12 shows clearly that the damage index in y direction (DI_y) is larger than that in x direction (DI_x). Moreover, compared to DI_x , DI_y experiences an obvious increasing trend with the increase of earthquake intensity, especially from 0.60 g to 0.96 g PGA. These results can be ascribed to the effect of resonance, which happened in the y direction during the earthquake excitation, and the specimen is more venerable in y direction than that in x direction. However, numerical results show that almost no damage ($DI < 0.1$) happens in both x and y directions when subjected to the PGA below 0.96 g of earthquakes. Therefore, it illustrates that the seismic performance of specimens can withstand more severe earthquakes (e.g., PGA > 0.96 g for this specimen or PGA > 0.32 g for prototype linked to the similarity relationships) (Table 2). Moreover, this numerical result also proves the experimental result detailed in Section 3.1.

6. Parameters Analysis

Due to the acceleration limits of shake tables, the maximum earthquake intensities used by shaking table tests were no more than 0.96 g PGA. Therefore, the seismic responses and damage level of specimen under more severe earthquakes (e.g., PGA > 0.96 g) were still unclear. To address this challenge, parameters analyses with different earthquake intensities (i.e., from 1.05 g to 1.95 g) were conducted using this validated FE model. The numerical results can be beneficial to safer seismic design of the corresponding prototype pier linked to the similarity relationships (Table 2).

6.1. Acceleration. Figure 13 gives the comparison of the maximum absolute acceleration (in x and y directions) when the specimen is subjected to different earthquake intensities (from 1.05 g to 1.95 g). Numerical results show that the accelerations at the top of specimen increase with the increase of earthquake intensity. Specifically, the maximum absolute acceleration increases from 1.4 g to 2.3 g (x direction) and 2.3 g to 3.2 g (y direction). Moreover, due to the difference in bending stiffness between the specimen in x and y directions (i.e., $EI_x < EI_y$), the maximum absolute acceleration at the top of specimen in y direction (A_y) is larger than that in x direction (A_x). This result means that the vibration of specimen is more easily affected in the y direction when subjected to an earthquake.

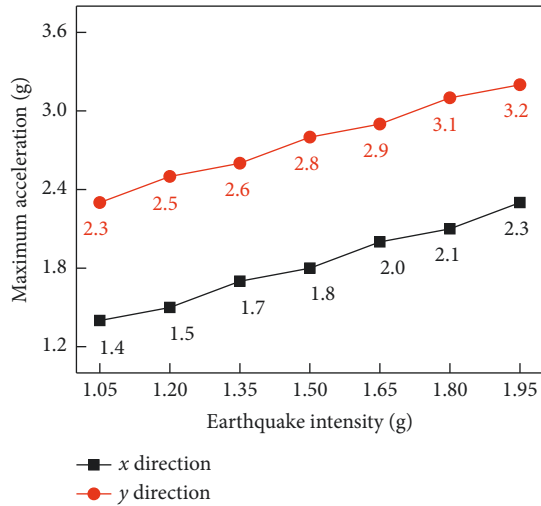


FIGURE 13: Comparison of maximum acceleration under different earthquake excitations.

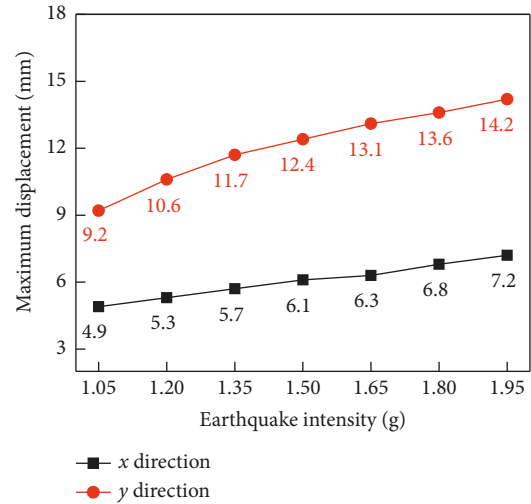


FIGURE 15: Comparison of maximum absolute displacement (in x and y directions) at the top of specimen.

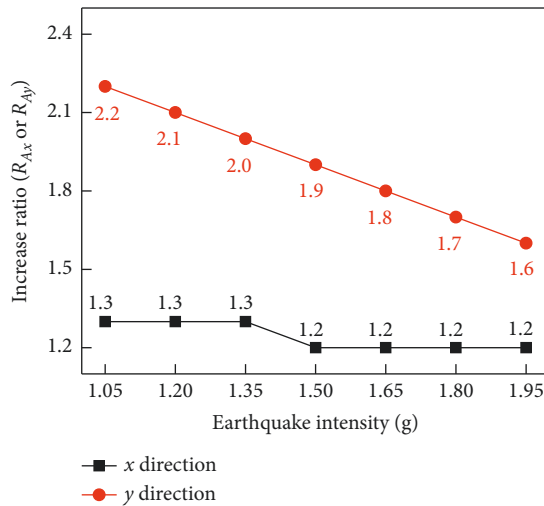


FIGURE 14: Comparison of acceleration increase ratio under different earthquake excitations.

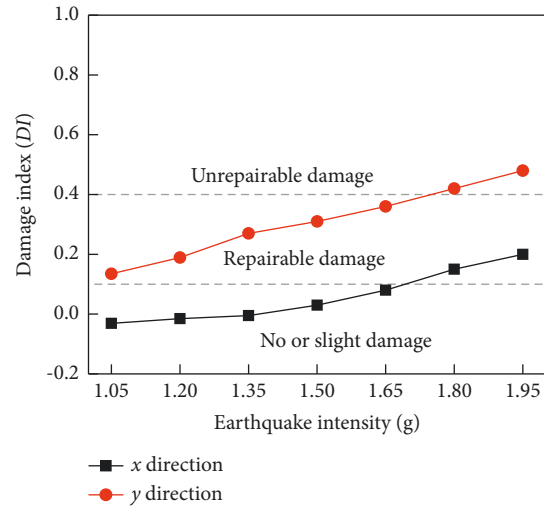


FIGURE 16: Variation of specimen damage indices with earthquake intensity.

In addition, to study the effect of earthquake intensity on the acceleration response, the ratio of maximum absolute acceleration recorded at the top of the specimen in the x or y directions (i.e., A_x or A_y) to the PGA (A_g) is used and denoted as R_{Ax} (A_x/A_g) (or R_{Ay} (A_y/A_g)). The calculation result (Figure 14) shows that both R_{Ax} and R_{Ay} experience a decreasing trend with the increase of earthquake intensity (from 1.05 g to 1.95 g). This can be reasonably explained by the fact that the earthquake damage of this specimen developed with the increase of earthquake intensity. Therefore, the bending stiffness of specimen in both x (EI_x) and y (EI_y) directions is reduced, resulting in a decreasing trend in R_{Ax} and R_{Ay} . However, due to the effect of resonance (discussed in Section 3.3), the earthquake damage of specimen in y direction is larger than that in x direction. Therefore, compared to a tiny decrease in R_{Ax} (from 1.3 to 1.2), a relatively obvious decreasing trend can be found in R_{Ay} (from 2.2 to 1.6).

6.2. Displacement. The comparison of maximum absolute displacement at the top of when subjected to the earthquakes (from 1.05 g to 1.95 g PGA) is studied (Figure 15) in this section. It can be seen that the maximum absolute displacement in y direction (D_y) is larger than that in x direction (D_x). To be specific, the maximum absolute displacement increases from 4.9 mm to 7.2 mm in x direction and from 9.2 mm to 14.2 mm in y direction. Numerical results show that the displacement in y direction is about twice that in x direction and therefore, seismic protection (e.g., prevention of girder falling off) of this specimen should pay more attention to the displacement response in y direction (transverse).

6.3. Earthquake Damage Level. Figure 16 illustrates the damage level of specimen subjected to these earthquakes (PGA from 1.05 g to 1.95 g). It shows clearly that both DI_x and DI_y experience an increasing trend with the increase

of earthquake intensity. However, the damage level of this specimen is different in x and y directions. To be specific, the specimen in x direction shows no or slight damage ($DI < 0.1$) when the earthquake intensity increases from 1.05 g to 1.65 g, while repairable damage ($0.1 < DI < 0.4$) can be found in y direction within this intensity range. Finally, repairable and unreparable damage can be seen in x and y directions, respectively, as the earthquake intensity increases to 1.95 g PGA. Numerical results demonstrate the different damage level of specimen under these earthquake excitations and therefore, researchers can take good use of these findings for better earthquake design or protection of this type of HSRB pier in the future.

7. Conclusions

9 scaled high-speed railway bridge pier specimens with rounded rectangular cross section were conducted and tested under the experimental earthquake excitations (0.45 g, 0.60 g, and 0.96 g, according to the similarity relationship illustrated in this work). The acceleration, displacement, and change of natural frequency of specimens were observed from the tests. Moreover, FE model of specimens was established and validated by the experiments. The hysteretic behavior and damage level of specimens under these earthquakes were also studied using FE model. In addition, parameter analyses were conducted using this validated FE model to study the seismic performance and damage level of this specimen under more severe earthquake intensities (from 1.05 g to 1.95 g). To be specific, the following conclusions can be drawn from this study:

- (1) The experimental results show that the change of first natural frequency of specimen before and after all earthquake scenarios was not obvious (about 6.8% and 8.3% for x and y directions, respectively). Therefore, this specimen remains slightly damaged for all experimental earthquake scenarios (from 0.45 g to 0.96 g).
- (2) Finite element (FE) model of specimens was established and validated. Parameter analyses with more severe earthquake intensities (from 1.05 g to 1.95 g) were also conducted using validated FE model. Results show that the maximum absolute acceleration at the top of specimen increases from 1.4 g to 2.3 g (transverse direction) and 2.3 g to 3.2 g (longitudinal direction). Moreover, the maximum absolute displacement increases from 4.9 mm to 7.2 mm (transverse direction) and from 9.2 mm to 14.2 mm (longitudinal direction). All these numerical results show that the effect of earthquake intensity to the earthquake response of specimen in longitudinal direction is more obvious than that in transverse direction. Therefore, the vibration of specimen is more easily affected in the longitudinal direction and seismic design should pay attention to this.

- (3) Numerical results demonstrate the different damage level of specimen under severe earthquake excitations (from 1.05 g to 1.95 g). Specifically, the specimen in transverse direction shows no or slight damage ($DI < 0.1$), while repairable damage ($0.1 < DI < 0.4$) can be seen in longitudinal direction as the earthquake peak ground acceleration increases from 1.05 g to 1.65 g. Finally, repairable and unreparable damage can be seen in transverse and longitudinal directions, respectively, as the earthquake intensity increases to 1.95 g.

Data Availability

Some or all data, models, or code that support the findings of this study are available from the corresponding author upon reasonable request.

Conflicts of Interest

The authors declare that there are no conflicts of interest regarding the publication of this paper.

Acknowledgments

This research was supported by the Special Fund of Strategic Leader in Central South University (grant no. 2016CSU001) and Hunan Construction Investment Group Co., Ltd. The second author is grateful to the Innovation-Driven Plan in Central South University (2022ZZTS0715).

References

- [1] L. Jiang, X. Kang, C. Li, and G. Shao, "Earthquake response of continuous girder bridge for high-speed railway: a shaking table test study," *Engineering Structures*, vol. 180, pp. 249–263, 2019.
- [2] X. Kang, L. Jiang, Y. Bai, and C. Caprani, "Seismic damage evaluation of high-speed railway bridge components under different intensities of earthquake excitations," *Engineering Structures*, vol. 152, pp. 116–128, 2017.
- [3] A. Monteiro, A. Arêde, and N. Vila Pouca, "Seismic behavior of coupled column bridge RC piers: experimental campaign," *Engineering Structures*, vol. 132, pp. 399–412, 2017.
- [4] A. V. Pinto, J. Molina, and G. Tsionis, "Cyclic tests on large-scale models of existing bridge piers with rectangular hollow cross-section," *Earthquake Engineering & Structural Dynamics*, vol. 32, no. 13, pp. 1995–2012.
- [5] Y. Chung, J. Park, and J. Seo, *Seismic Performance Evaluation of RC Bridge Piers Confined with Spiral FRP - (I) FRP Rope*, 2003.
- [6] Q. Han, X. Du, Y. Zhao, and L. Wang, "Cyclic testing on rectangular hollow bridge piers under axial load and biaxial bending," *China Journal of Highway and Transport*, vol. 26, no. 1, pp. 58–66, 2013.
- [7] Y. Yeh, Y. Mo, and C. Yang, "Full-scale tests on rectangular hollow bridge piers," *Materials and Structures*, vol. 35, no. 246, pp. 117–125, 2002.
- [8] Z. Xia, Z. Zong, and R. Zhong, "Seismic performance of reinforced concrete thin-walled piers with rectangular hollow cross-sections based on bi-axial quasi-static testing," *Journal of Southeast University (Natural Science Edition)*, vol. 43, no. 1, pp. 180–187, 2013.

- [9] C. Shim, C. Chung, and H. Kim, "Experimental evaluation of seismic performance of precast segmental bridge piers with a circular solid section," *Engineering Structures*, vol. 30, no. 12, pp. 3782–3792, 2008.
- [10] Z. Wang, W. Sui, Z. Zhao, H. Pang, and J. Liao, "Study on seismic performance of partially concrete-filled steel circular bridge piers with transverse diaphragm," *Journal of Building Structures*, vol. 34, no. S1, pp. 233–239, 2013.
- [11] K. Osada, T. Yamaguchi, and S. Ikeda, "Seismic performance and the strengthening of hollow circular RC piers having reinforcement cut-off planes and variable wall thickness," *Transactions of the Japan Concrete Institute*, vol. 21, no. 1, pp. 263–274, 2000.
- [12] H. Yuan, J. Dang, and T. Aoki, "Behavior of partially concrete-filled steel tube bridge piers under bi-directional seismic excitations," *Journal of Constructional Steel Research*, vol. 93, pp. 44–54, 2014.
- [13] Z. Dong, Q. Han, and D. Xiu-Li, "Analytical model and experimental validation of FRP confined bridge columns with RC rectangular hollow cross sections," *Engineering Mechanics*, 2013.
- [14] D. Lee, E. Choi, and G. Zi, "Evaluation of earthquake deformation and performance for RC bridge piers," *Engineering Structures*, vol. 27, no. 10, pp. 1451–1464, 2005.
- [15] J. Guo, K. Xin, M. He, and L. Hu, "Experimental study and analysis on the seismic performance of a self-centering bridge pier," *Engineering Mechanics*, 2012.
- [16] Z. Sun, B. Si, D. Wang, and X. Guo, "Experimental research and finite element analysis of bridge piers failed in flexure-shear modes," *Earthquake Engineering and Engineering Vibration*, vol. 7, no. 4, pp. 403–414, 2008.
- [17] Y. Hu and W. Guo, "Seismic response of high-speed railway bridge-track system considering unequal-height pier configurations," *Soil Dynamics and Earthquake Engineering*, vol. 137, Article ID 106250, 2020.
- [18] H. Krawinkler and P. Moncarz, "Theory and application of experimental model analysis in earthquake engineering," *Stanford University*, 1981.
- [19] Y. Zhou and X. Lv, "Method and technology for shaking table model test of building structures," 2012.
- [20] Y. Zhou, L. Wensheng, and L. Xilin, "Practical model design method of shaking table tests," *Structural Engineers*, 2003.
- [21] L. Jiang, X. Kang, and L. Chen, "Mega-earthquake response of benchmark high-speed rail bridge piers based on shaking table tests," *Engineering Failure Analysis*, vol. 140, Article ID 106608, 2022.
- [22] OpenSees, *OpenSees User's Guide*, 2022.
- [23] D. Kent and R. Park, "Flexural members with confined concrete," *Journal of the Structural Division*, vol. 97, no. 7, pp. 1969–1990.
- [24] B. Scott, R. Park, and M. Priestley, "Stress-strain behavior of concrete confined by overlapping hoops at low and high strain rates," *Aci Journal*, vol. 79, no. 1, pp. 13–27, 1982.
- [25] J. Mander, M. Priestley, and R. Park, "Theoretical stress-strain model for confined concrete," *Journal of Structural Engineering*, vol. 114, no. 8, pp. 1804–1826, 1988.
- [26] M. Menegotto, "Method of analysis of cyclically loaded RC plane frames including changes in geometry and non-elastic behavior of elements under normal force and bending," *Preliminary Report labse*, vol. 13, 1973.
- [27] W. Stone and A. Taylor, "Seismic performance of circular bridge columns designed in accordance with AASHTO/CALTRANS standards," *Concrete Bridges*, vol. 170, 1993.